www.sciencemag.org/cgi/content/full/science.aab4070/DC1

Supplementary Materials for

Structure of *Tetrahymena* telomerase reveals previously unknown subunits, functions, and interactions

Jiansen Jiang, Henry Chan, Darian D. Cash, Edward J. Miracco, Rachel R. Ogorzalek Loo, Heather E. Upton, Duilio Cascio, Reid O'Brien Johnson, Kathleen Collins, Joseph A. Loo, Z. Hong Zhou, Juli Feigon*

*Corresponding author. E-mail: feigon@mbi.ucla.edu

Published 15 October 2015 on *Science* Express
DOI: 10.1126/science.aab4070

This PDF file includes:

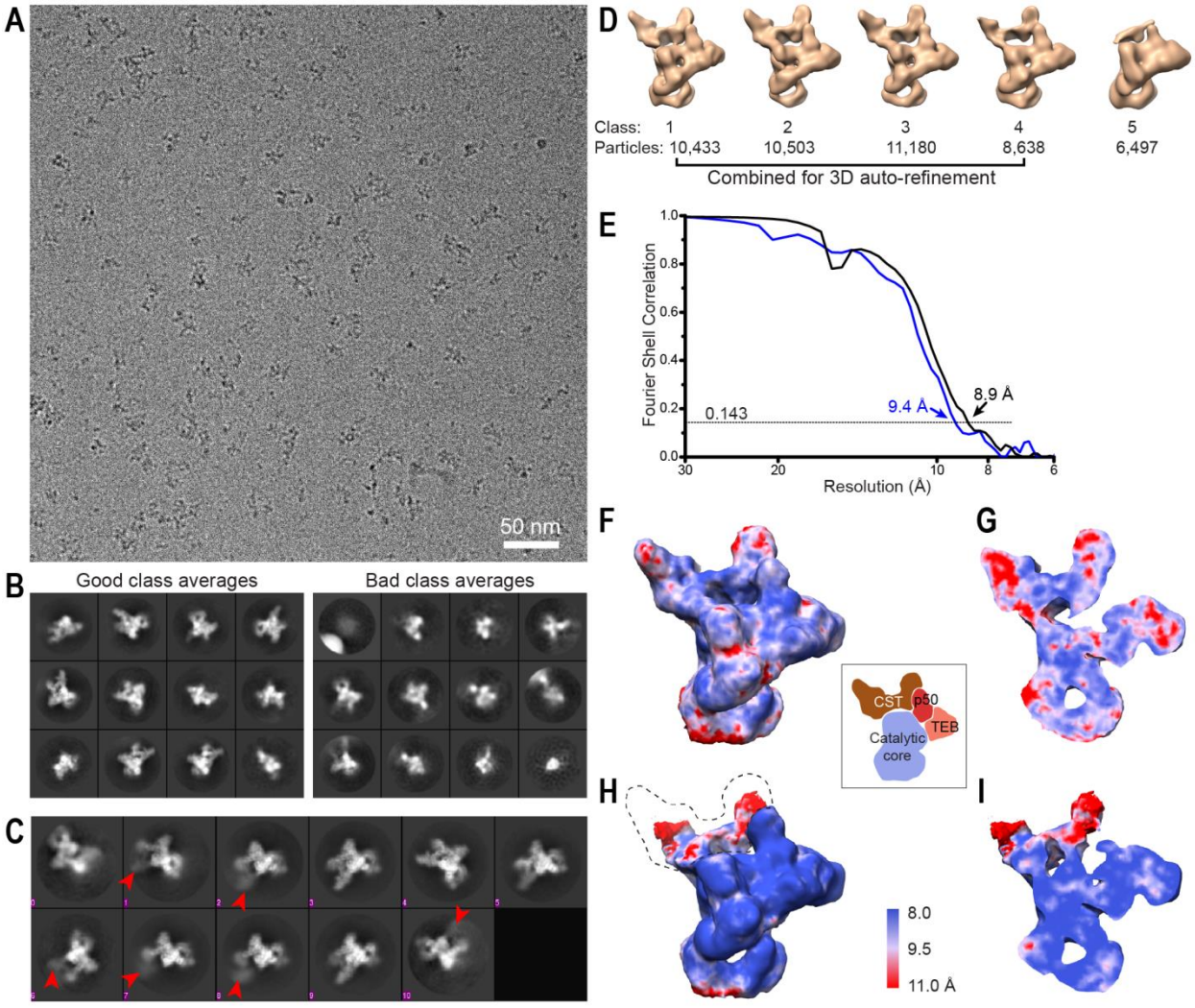

Fig. S1. Cryo-EM of *Tetrahymena* telomerase holoenzyme and resolution estimation. (**A**) A full-size (3710 × 3710 pixels) drift-corrected cryo-EM micrograph of *Tetrahymena* telomerase holoenzyme acquired at -4.9 µm defocus. (**B**) Representative cryo-EM 2D class averages of particles that are assessed as 'good' (left) or 'bad' (right) classes by visual inspection during data processing. (**C**) Cryo-EM 2D class averages of front-view particles. Red arrowheads depict the missing or fuzzy density of the flexible p75-p45-p19 subcomplex. The side length of each image box in (B) and (C) is 35 nm. (**D**) Cryo-EM 3D reconstructions generated by 3D classification. The density for p75-p45-p19 is missing in class 5 due to its flexibility. The particles sorted to the classes (1-4) that show an intact holoenzyme structure were combined together for the 3D auto-refinement. (**E**) 'Gold standard' FSC curves between two independently refined maps from the 3D auto-refinement that were carried out with a spherical mask including all subunits (blue) or with a soft-edge mask excluding p75-p45-p19 subcomplex (black). Each FSC curve was calculated with an auto-mask that was corrected by phase randomization. The resolutions were estimated at the 0.143 criterion. (**F-I**) Surface views (F, H) and cut-through views (G, I) of the unsharpened cryo-EM maps refined with a spherical mask (F, G) and with a soft-edge mask excluding the p75-p45-p19 subcomplex (H, I). The cryo-EM maps are colored by local

resolution estimated by ResMap using two cryo-EM maps independently refined from halves of data. The region corresponding to the masked p75-p45-p19 is depicted by the dashed line in (H). The inset is the schematic of the subcomplex organization shown in the same view as the local resolution maps.

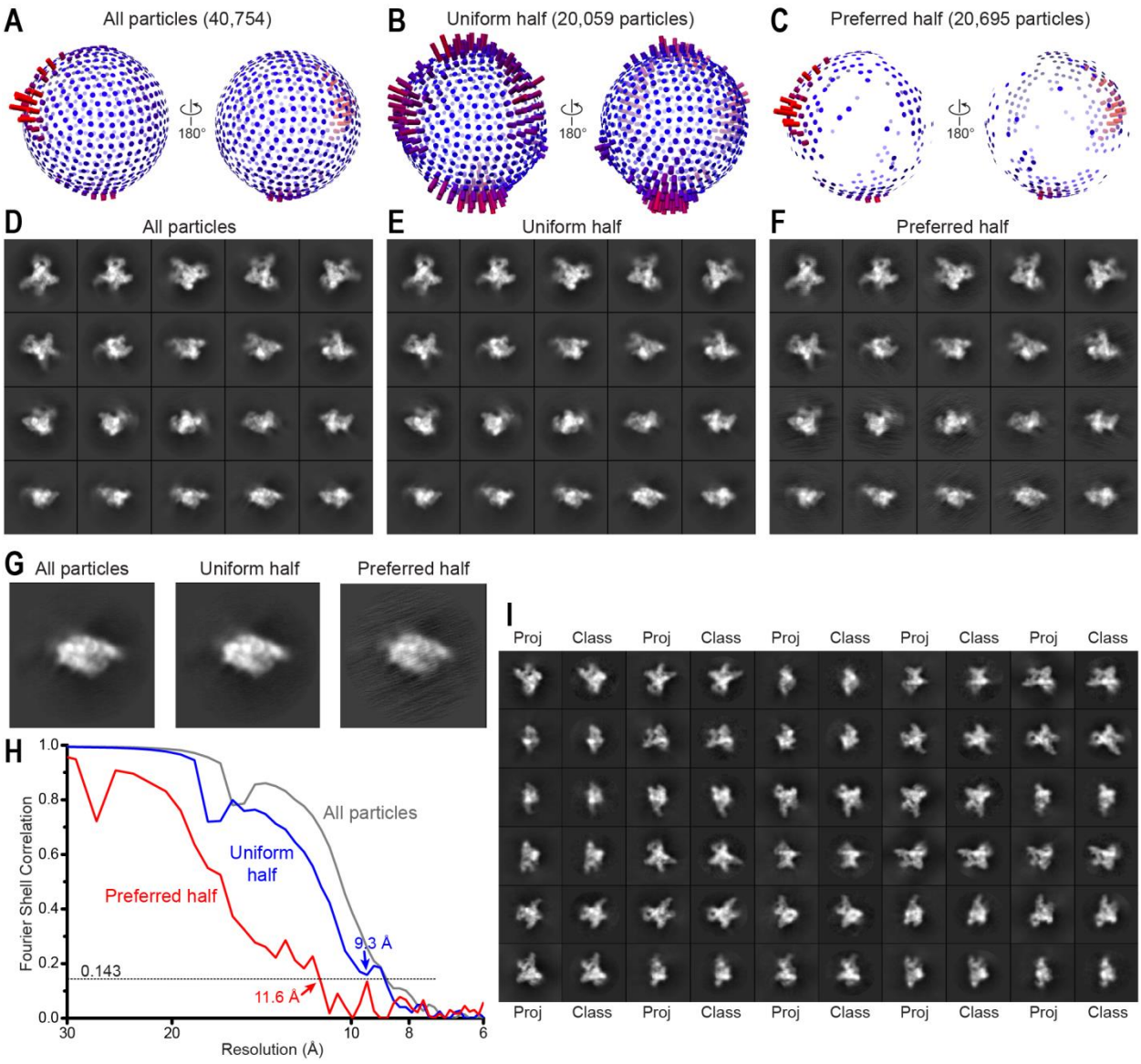

Fig. S2. Assessment of orientation distribution of *Tetrahymena* telomerase holoenzyme particles and its impact on reconstruction resolution. (**A-C**) Euler angle distributions, generated by RELION 3D auto-refinement, of all particles (**A**) used in the 8.9-Å reconstruction, the half of all particles that are more uniformly distributed ('uniform half') (**B**), and the other half that show strongly preferred orientation ('preferred half') (**C**). Note the histograms show relative particle counts at different orientations within each data set and are not comparable across data sets for absolute particle counts. The 3D auto-refinements of three data sets were all carried out with a soft-edge mask excluding p75-p45-p19 subcomplex using the same parameters in RELION. (**D-F**) Projections (30° interval) of the unfiltered 3D reconstructions from all particles, the 'uniform half', and the 'preferred half'. Some projections from the 'preferred half' (F) show striped artifacts resulting from missing information; the projections from all particles (D) and the 'uniform half' (E) are isotropic without the artifacts, indicating that the quality of reconstruction from all particles or the 'uniform half' was not degraded by the problem of preferred orientation existing in the 'preferred half'. (**G**) Close-up view of representative

projections that show striped artifacts from the ‘preferred half’ but not from all particles or the ‘uniform half’. (**H**) ‘Gold standard’ FSC curves of the refinements using all particles (grey), the ‘uniform half’ (blue), and the ‘preferred half’ (red). (**I**) Comparison of representative projections (‘Proj’) from the 9.4-Å cryo-EM map and the corresponding class averages (‘Class’). The side length of each image box in (D-G and I) is 35 nm.

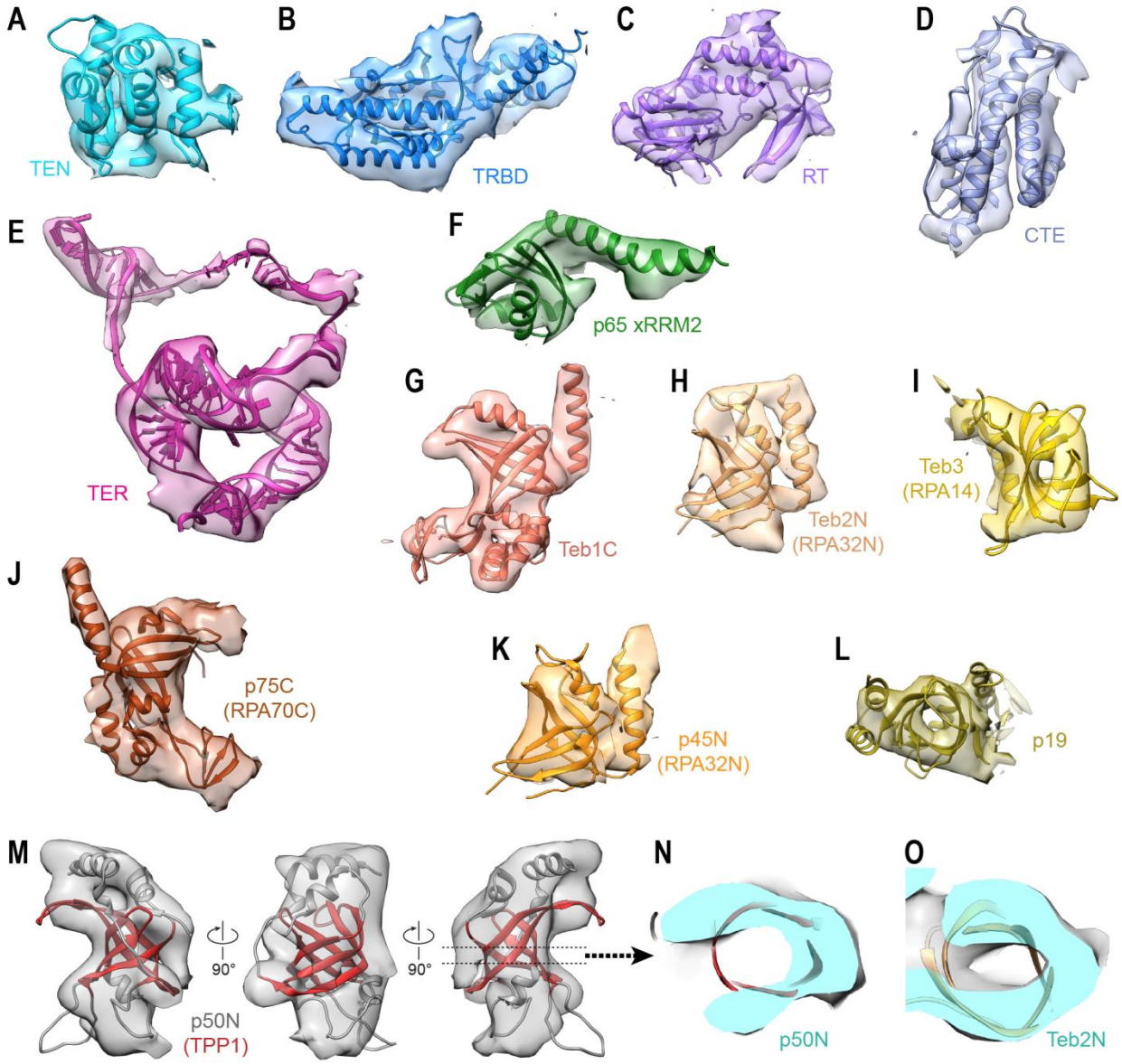

Fig. S3. Fitting of atomic structures or homology models in the cryo-EM maps. (**A-M**) Fitting of TERT (**A**) TEN, (**B**) TRBD, (**C**) homology model of RT and (**D**) homology model of CTE, (**E**) TER, (**F**) p65 xRRM2, (**G**) Teb1C, (**H**) RPA32N for Teb2N, (**I**) RPA14 for Teb3, (**J**) RPA70C for p75C, (**K**) RPA32N for p45N, and (**L**) p19, (**M**) TPP1 for p50N. Three views are shown to illustrate good fit of OB-fold β-barrel (red); loops and helices are in gray. (**N, O**) Horizontal cross section through density of (**N**) p50N and (**O**) Teb2N to show the hole in the density corresponding to the center of the OB-fold β-barrel. The atomic or homology models used in the fitting are summarized in table S1. Atomic or homology models are shown as ribbons and cryo-EM maps are show as transparent surfaces. 8.9-Å and 9.4-Å cryo-EM maps are used in (A-I, M-O) and (J-L), respectively.

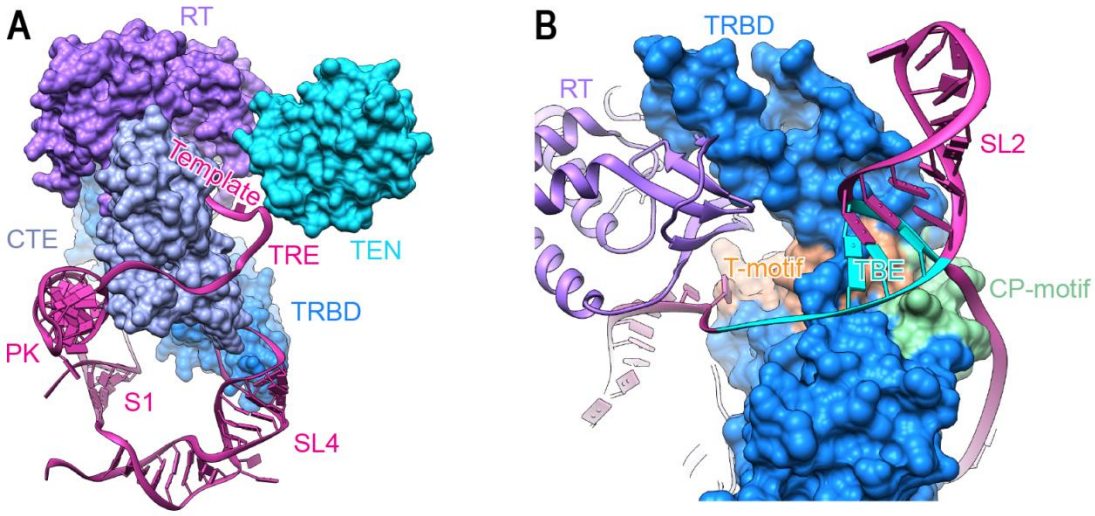

Fig. S4. Model of the TERT-TER complex. (**A**) Front view of TERT-TER complex illustrating the positions of the PK and template on opposite sides of TERT ring, the TEN domain, and the TRE between the TERT ring and TEN domain, with possible contact to TEN. (**B**) Close-up view of the interaction between TER SL2/TBE and TERT TRBD illustrating the location of TBE single-strand nts on either side of TERT ring near CP motif. The T and CP motif of TRBD and TER TBE are colored in brown, green, and cyan, respectively.

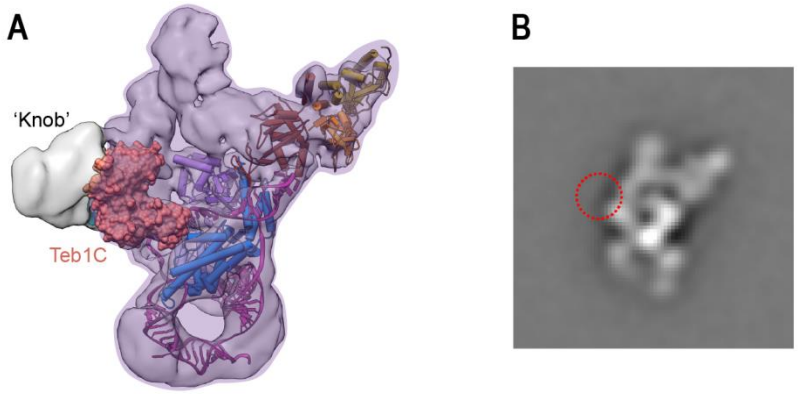

Fig. S5. The cryo-EM density of the newly discovered proteins Teb2 and Teb3. (**A**) "Back view" of the 9.4-Å cryo-EM map fit with known structures (ribbons and space-fill model). The cryo-EM density assigned to previously known subunits is superimposed with a shade of purple. Based on exhaustive fitting of available atomic models and visual inspection, the "knob" density does not correspond to any previously identified subunits. (**B**) Negative-stain EM class average of p50-F telomerase. Sample preparation, data acquisition, and processing have been described previously (*29*). Red dashed circle marks the location of the missing "knob" density. The side length of the image box is 35 nm.

A. RPA32N-OB aligned with Teb2N-OB

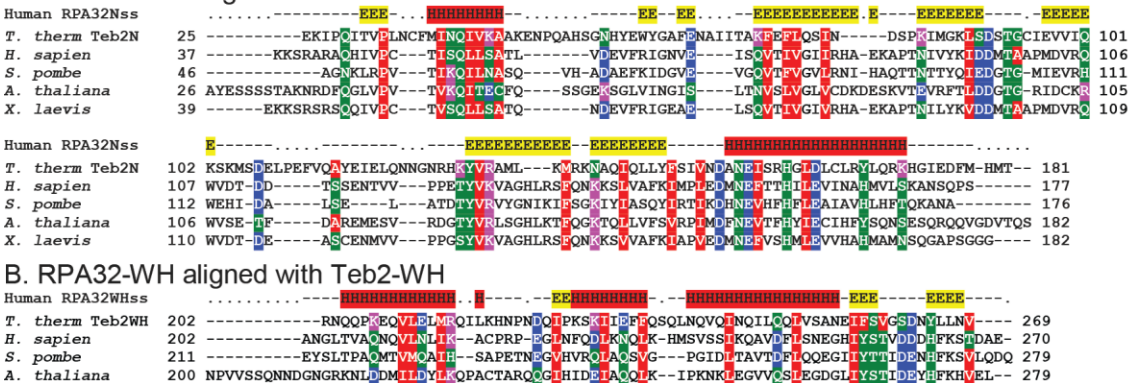

B. RPA32-WH aligned with Teb2-WH

C. RPA14 aligned with Teb3

D. Stn1N-OB aligned with p45N-OB

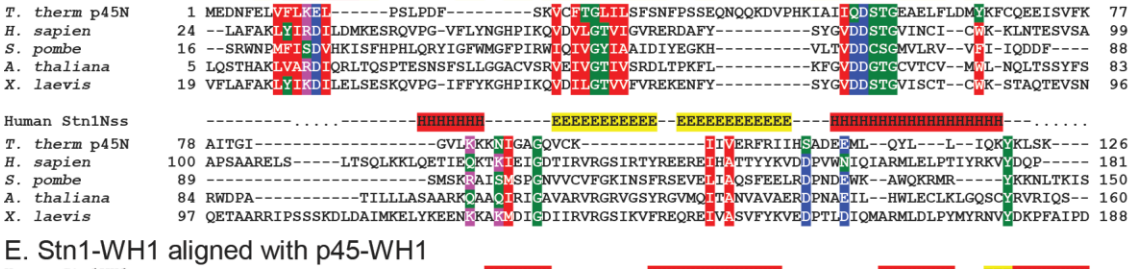

E. Stn1-WH1 aligned with p45-WH1

F. Stn1-WH2 aligned with p45-WH2

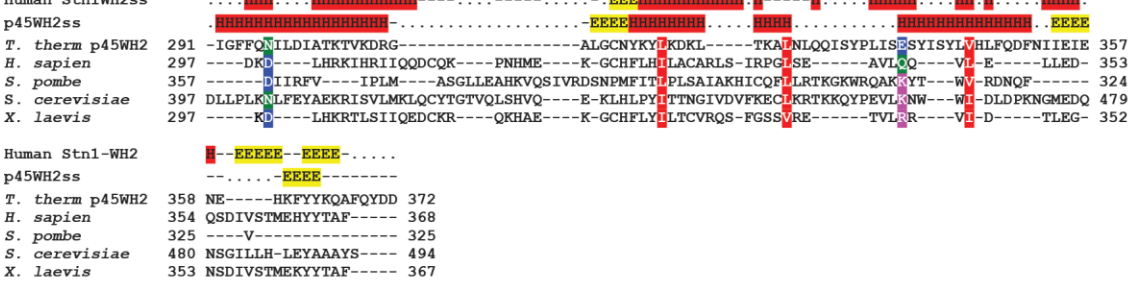

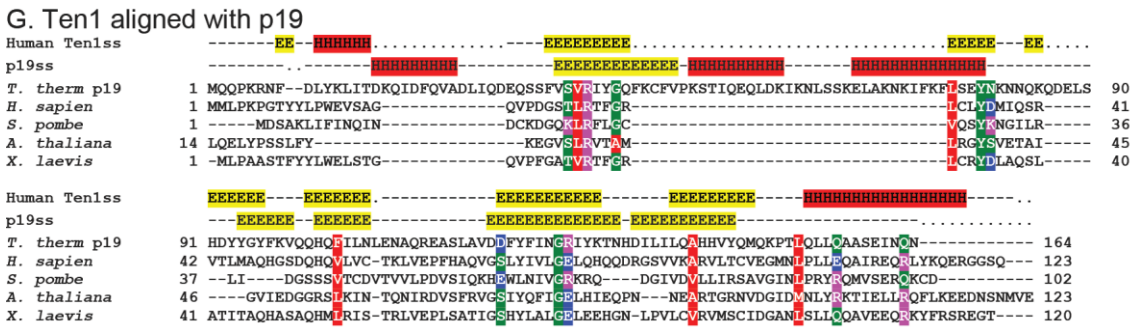

Fig. S6. Multiple sequence alignments of TEB2/3, RPA2/3, Stn1, Ten1, p45 and p19. Secondary structures from the previously reported crystal structures of human proteins and crystal structures of *Tetrahymena* proteins reported here (p45C WH1/WH2 and p19) are shown as "." for gaps, "-" for loops, "E" for beta-sheet, and "H" for alpha-helix. Conserved or similar residues are highlighted according to their chemical characteristics: hydrophobic, polar, negatively charged, positively charged. (**A**) RPA32N OB-fold aligned with Teb2N OB-fold. (**B**) RPA32 WH domain aligned with Teb2 WH domain. (**C**) RPA14 aligned with Teb3. (**D**) Stn1N OB-fold aligned with p45N OB-fold. (**E**) Stn1 WH1 domain aligned with p45 WH1 domain. (**F**) Stn1 WH2 domain aligned with p45 WH2 domain. (**G**) Ten1 aligned with p19. Alignments reveal close homology of Teb2/3 with RPA2/3. Consistent with previous observations of low sequence homology of Stn1 and Ten1 across kingdoms, p45 and p19 show lower sequence homology with Stn1 and Ten1 proteins. Multiple sequence alignments were performed using CLUSTAL.

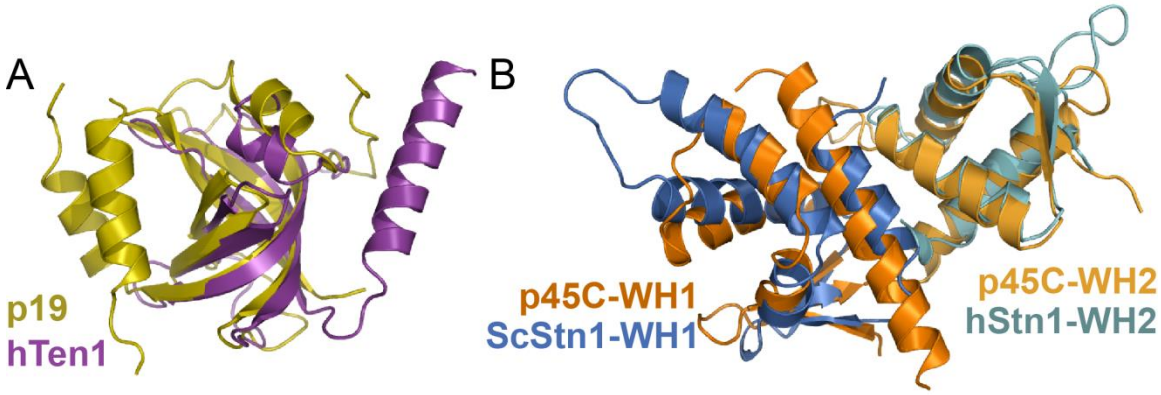

Fig. S7. p19 and p45C are structurally similar to Ten1 and Stn1C. (**A**) Structural alignment of p19 (yellow) with human Ten1 [PDB 4JOI] (purple). RMSD = 2.5Å. (**B**) Structural alignment of p45 WH1 (orange) and WH2 (yellow-orange) domains with *S. cerevisiae* Stn1C-WH1 [PDB 3KEY] (blue) and human Stn1C-WH2 [PDB 4JQF] (teal), respectively. RMSD = 2.8 and 1.9, respectively. Structural alignments were made using the Dali server (http://ekhidna.biocenter.helsinki.fi/dali_server**).**

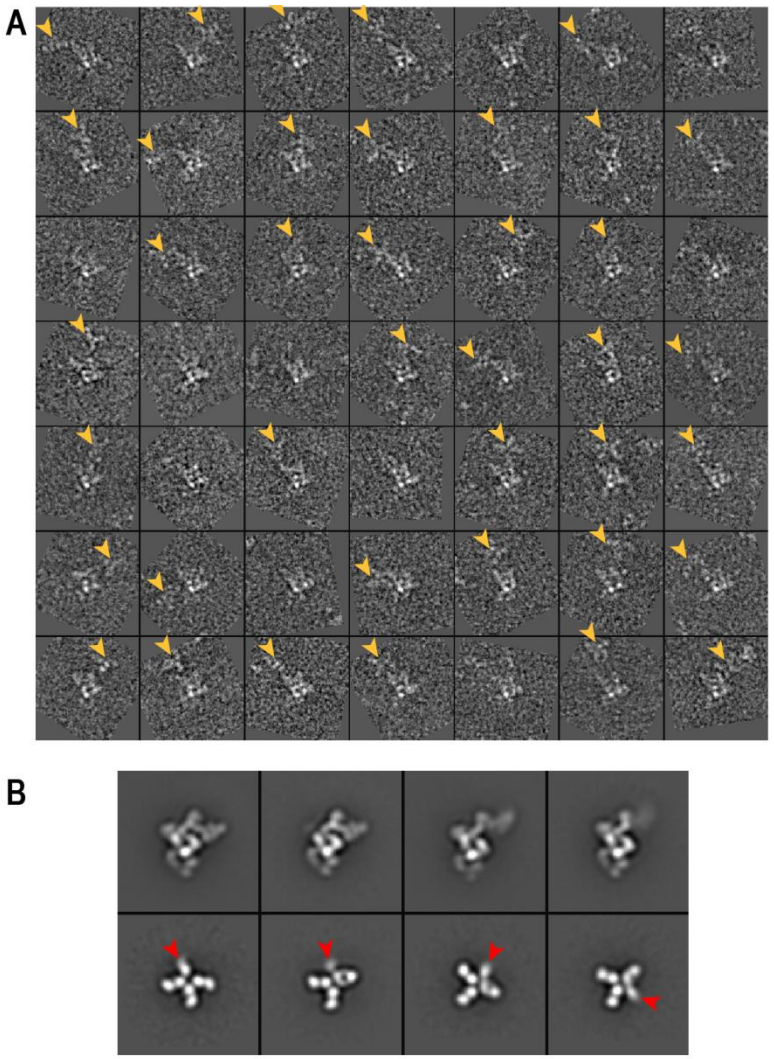

Fig. S8. Fab-labeled p45-F telomerase holoenzyme. (**A**) Randomly selected negative-stain EM particle images of telomerase homoenzyme with the C-terminus of p45-F labeled with anti-FLAG Fab. Distinguishable densities of Fab are marked with yellow arrowheads. Particles are rotated to match the orientation of telomerase holoenzyme among them for the ease of visualization. The Fab density mostly appears in the top-left corner of the image that is near the position of p45N. (**B**) Negative-stain EM class averages of Fab-labeled p45-F telomerase holoenzyme particles. Two families of class averages are observed: telomerase holoenzyme (first row) and 3 Fab attached to the C-terminus of p45 (second row). Red arrowheads mark the density of the C-terminal domain of p45. No class averages show these two structures together due to the flexible positioning between them, attributed to unstructured linker residues. The side length of each image box in (A) and (B) is 56 nm and 42 nm, respectively. Sample preparation, data acquisition, and processing have been described previously (*29*).

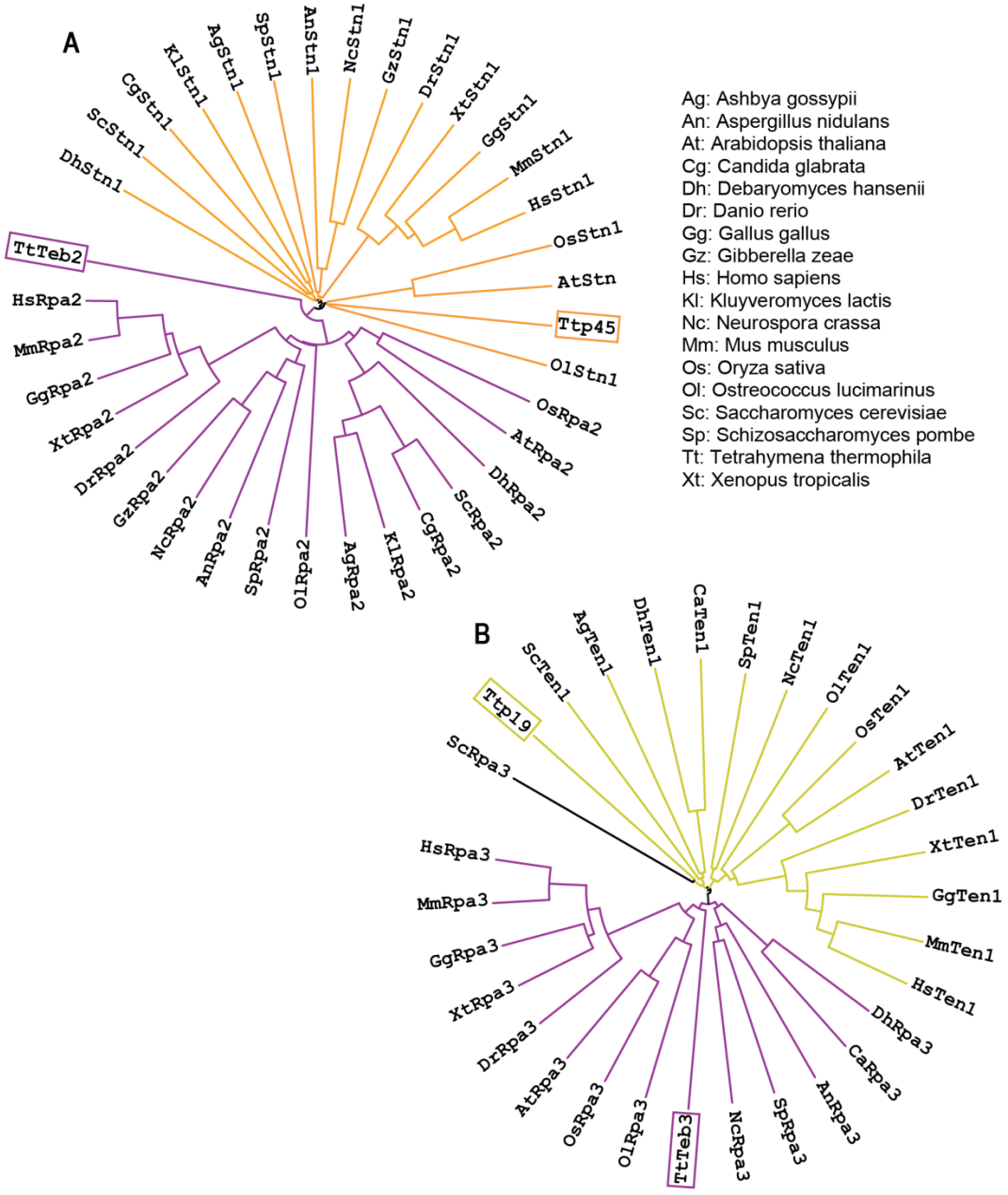

Fig. S9. Phylogenetic cluster analysis of Stn1/Rpa2 and Ten1/Rpa3. (**A**) Stn1 and Rpa2 and (**B**) Ten1 and Rpa3 cluster in distinct monophyletic groups. Shown is a rooted maximum likelihood phylogeny of Stn1 and Rpa2 (A) and Ten1 and Rpa3 (B) inferred using the WAG amino-acid transition model in RAxML [A. Stamatakis: "RAxML Version 8: A tool for Phylogenetic Analysis and Post-Analysis of Large Phylogenies" in *Bioinformatics*, **30**, 1312-1313, 2014] from sequence alignment generated with ClustalW2. Alignments of the two protein families were conducted simultaneously and the cluster analyses show that (A) p45 clusters with Stn1 while Teb2 clusters with Rpa2 and (B) p19 clusters with Ten1 while Teb3 clusters with Rpa3.

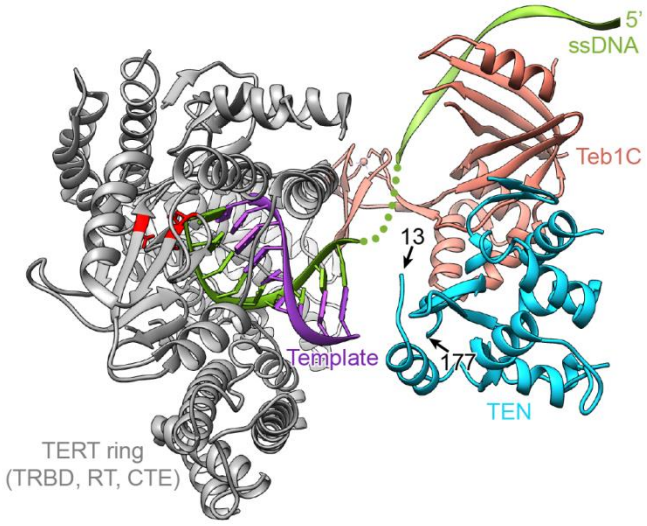

Fig. S10. Model of ssDNA exiting the template. Models of DNA (green) paired with the template (purple) and bound to Teb1C are based on the fitting of the crystal structures of *Tribolium* TERT (PDB ID: 3KYL) and RPA:ssDNA complex (PDB ID: 4GNX), respectively. The green dots indicate the region connecting the ssDNA from the two model structures. The N- and C-termini of the crystal structure of TEN are depicted by its amino acid numbers. TERT ring is in gray, active site catalytic triad residues are shown in red, and TEN is in cyan.

Table S1. X-ray crystal and NMR structures used in the fitting of the cryo-EM maps of *Tetrahymena* telomerase holoenzyme

Subunit	Domain	Structure fitted in the cryo-EM maps	Related PDB ID	Ref
TERT	TEN	*Tetrahymena* TERT TEN	2B2A	(*32*)
	TRBD	*Tetrahymena* TERT TRBD	2R4G	(*37*)
	RT	Homology model derived from *Tribolium* TERT	3DU6	(*31*)
	CTE	Homology model derived from *Tribolium* TERT	3DU6	(*31*)
TER	SL4	Model derived from *Tetrahymena* p65 xRRM2/TER S4 complex and L4	4ERD, 2M21	(*29, 33, 85*)
	SL2	*Tetrahymena* TER SL2	2M22	(*29, 86*)
	PK	*Tetrahymena* TER PK	2N6Q	this work
	Template	Homology model derived from *Tribolium* TERT/RNA-DNA hybrid complex	3KYL	(*38*)
	S1	Ideal A-form RNA helix	--	--
p65	xRRM2	p65 xRRM2/TER S4 complex	4ERD	(*33*)
p65	La+RRM1	hLa complex	2VOP	(*33, 87*)
Teb1	C	*Tetrahymena* Teb1C	3U50	(*50*)
Teb2	N	RPA32N in human RPA trimer	1L1O	(*51*)
Teb3		RPA14 in human RPA trimer	1L1O	(*51*)
p75	C	RPA70C in human RPA trimer	1L1O	(*51*)
p45	N	RPA32N in human RPA trimer	1L1O	(*51*)
p19		*Tetrahymena* p19	5DFM	this work
p50	N	Human TPP1	2I46	(*13*)
Telomere ssDNA		*Tribolium* TERT/RNA-DNA hybrid and fungal RPA/ssDNA complexes	3KYL, 4GNX	(*38, 88*)

Table S2A. Telomerase proteins identified from TERT-FZZ telomerase preparations by LC-MS/MS

			Replicate 1				Replicate 2				Replicate 3			
TTHERM ID	Protein	MW (kDa)	Uni. Pep[a]	Sig. Pep[b]	% Cov[c]	Score[d]	Uni. Pep[a]	Sig. Pep[b]	% Cov[c]	Score[d]	Uni. Pep[a]	Sig. Pep[b]	% Cov[c]	Score[d]
00112560	TERT	134.1	30	22	22	393	84	70	53	2440	37	22	30	370
000318539	p65	64.6	22	17	41	300	49	42	62	1447	36	20	50	358
01049190	p50	50.3	14	8	29	276	27	26	45	2539	11	7	29	147
0059040	p75	74.3	21	10	24	150	42	31	50	955	28	15	40	437
0083360	p45	43.8	17	11	34	201	30	27	59	1475	14	7	33	198
00658760	p19	19.5	7	3	38	88	9	8	50	223	1	1	8	39
00218760	Teb1	82.6	12	7	15	148	18	15	21	1479	5	2	8	251
00113129	Teb2	31.1	9	7	42	414	15	13	49	858	8	5	35	334
00439320	Teb3	14.0	8	7	44	406	9	8	51	507	5	3	40	409

Table S2B. Telomerase proteins identified from ZZF-p50 telomerase preparations by LC-MS/MS

			Replicate 1				Replicate 2			
TTHERM ID	Protein	MW (kDa)	Uni. Pep[a]	Sig. Pep[b]	% Cov[c]	Score[d]	Uni. Pep[a]	Sig. Pep[b]	% Cov[c]	Score[d]
00112560	TERT	134.1	15	3	12	40	40	33	31	616
000318539	p65	64.6	7	3	12	74	36	29	47	828
01049190	p50	50.3	16	8	38	118	30	24	60	1218
0059040	p75	74.3	24	15	33	256	25	19	37	334
0083360	p45	43.8	12	6	27	128	20	15	50	746
00658760	p19	19.5	7	4	33	79	9	7	44	241
00218760	Teb1	82.6	0	0	-	-	0	0	-	-
00113129	Teb2	31.1	0	0	-	-	1	1	-	-
00439320	Teb3	14.0	0	0	-	-	0	0	-	-

[a]Number of unique peptide sequences identified at $\leq$ 10 ppm mass accuracy
[b]Number of unique peptide sequences identified with E-value < 0.05 (>95% confidence that the match was not random)
[c]Percentage of theoretical sequence covered by identified peptides
[d]Mascot score employing all peptides with E-value < 0.05

Table S3. X-Ray Data Collection and Refinement Statistics

	MBP-p19	P45C
Data Collection		
Space group	$P2_13$	F222
Unit cell dimensions		
a, b, c (Å)	150.60, 150.60, 150.60	88.03, 124.62, 173.77
α, β, γ (˚)	90.00, 90.00, 90.00	90.00, 90.00, 90.00
Reflections observed	993,498	101,012
Unique reflections	50,601	18,884
Multiplicity	19.6	5.3
Wavelength (Å)	0.9795	0.9791
Resolution (Å)	2.30	2.38
Highest Resolution Shell (Å)	2.30 – 2.36	2.38 – 2.45
R_{sym} (%)[a]	11.9 (103.3)	6.4 (72.8)
$R_{p.i.m.}$ (%)[b]	3.9 (30.4)	3.3 (30.7)
CC(1/2)	99.9 (90.0)	99.9 (86.7)
I/σ	19.4 (3.4)	14.1 (2.5)
Completeness (%)	99.9 (98.7)	97.8 (78.6)
Wilson B value (Å^2)	40.16	53.10
Refinement		
Resolution (Å)	86.89 – 2.30	86.89 – 2.38
Resolution (Å) (last shell)	2.30 – 2.33	2.38 – 2.45
Reflections used	50,569	18,334
R_{work}(%) / R_{free}(%)[c]	17.5 / 22.6; (22.7 / 31.4)	20.7 / 26.4; (32.9 / 41.5)
Protein molecules in Asymmetric Unit	2	2
Number of non-H atoms		
Protein	7784	2730
Non-protein	207	6
RMS Deviations		
Bond lengths (Å)	0.008	0.008
Bond angles (˚)	1.14	1.01
Average B-factor (Å^2)		
Protein atoms	45.2	62.8
Non-protein atoms	56.8	50.4
Ramachandran plot regions[c]		
Favored	97.2	98.19
Allowed	2.8	1.81
Outliers	0.00	0.00

Highest resolution shell shown in parenthesis

[a] $R_{sym} = 100 \times \Sigma(I\text{-}I(mean))^2 / \Sigma(I)^2$

[b] $R_{p.i.m.} = 100 \times \Sigma\sqrt{(1/(N-1))}\Sigma\ (I\text{-}I(mean)) / \Sigma(I)^2$

where I is the observed intensity of the reflection HKL and the sum is taken over all reflections HKL and N is the redundancy

[c] $R_{factor} = 100 \times \Sigma||F_{obs}| - |F_{calc}|| / \Sigma|F_{obs}|$

F_{calc} and F_{obs} are the calculated and observed structure factor amplitudes, respectively. R_{work} refers to the R_{factor} for the data utilized in the refinement and R_{free} refers to the R_{factor} for 5% of the reflections randomly chosen that were excluded from the refinement

[c] Percentage of residues in Ramachandran plot regions were determined using Molprobity (Chen et.al 2010).

Table S4. NMR restraints and structure statistics for *Tetrahymena* TER pseudoknot

Parameter	Value
NMR distance and dihedral restraints	
Distance restraints	
Total NOEs	414
Intraresidue NOEs	103
Interresidue NOEs	311
Sequential (|i-j|) = 1	176
Long range (|i-j|) > 1	135
Hydrogen bond restraints*	82
Total dihedral angle restraints	171
Sugar pucker	140
χ	31
RDCs	79
Structure statistics	
Violations (mean ± SD)	
Distance constraints (Å)	0.054 ± .001
Dihedral angle constraints (°)	0.020 ± .002
Maximum dihedral angle violation (°)	2.03
Maximum distance violation (°)	0.29
Deviations from idealized geometry	
Bond lengths (Å)	0.0057 ± .0001
Bond angles (°)	0.95 ± .02
Impropers (°)	0.61 ± .04
Average pairwise rmsd (Å) **	
Heavy	0.83 ± 0.23
Backbone	0.84 ± 0.24

* Two hydrogen bond restraints were used for each hydrogen bond.

** Pairwise RMSD was calculated for the lowest 10 energy structures.

References and Notes

1. E. H. Blackburn, C. W. Greider, J. W. Szostak, Telomeres and telomerase: The path from maize, *Tetrahymena* and yeast to human cancer and aging. *Nat. Med.* **12**, 1133–1138 (2006). Medline doi:10.1038/nm1006-1133

2. E. H. Blackburn, K. Collins, Telomerase: An RNP enzyme synthesizes DNA. *Cold Spring Harbor Perspect. Biol.* **3**, a003558 (2011). Medline doi:10.1101/cshperspect.a003558

3. M. Armanios, E. H. Blackburn, The telomere syndromes. *Nat. Rev. Genet.* **13**, 693–704 (2012). Medline doi:10.1038/nrg3246

4. B. Bernardes de Jesus, M. A. Blasco, Telomerase at the intersection of cancer and aging. *Trends Genet.* **29**, 513–520 (2013). Medline doi:10.1016/j.tig.2013.06.007

5. S. E. Artandi, R. A. DePinho, Telomeres and telomerase in cancer. *Carcinogenesis* **31**, 9–18 (2010). Medline doi:10.1093/carcin/bgp268

6. J. Nandakumar, T. R. Cech, Finding the end: Recruitment of telomerase to telomeres. *Nat. Rev. Mol. Cell Biol.* **14**, 69–82 (2013). Medline doi:10.1038/nrm3505

7. J. A. Stewart, M. F. Chaiken, F. Wang, C. M. Price, Maintaining the end: Roles of telomere proteins in end-protection, telomere replication and length regulation. *Mutat. Res.* **730**, 12–19 (2012). Medline doi:10.1016/j.mrfmmm.2011.08.011

8. L. Y. Chen, J. Lingner, CST for the grand finale of telomere replication. *Nucleus* **4**, 277–282 (2013). Medline doi:10.4161/nucl.25701

9. F. L. Zhong, L. F. Batista, A. Freund, M. F. Pech, A. S. Venteicher, S. E. Artandi, TPP1 OB-fold domain controls telomere maintenance by recruiting telomerase to chromosome ends. *Cell* **150**, 481–494 (2012). Medline doi:10.1016/j.cell.2012.07.012

10. A. N. Sexton, D. T. Youmans, K. Collins, Specificity requirements for human telomere protein interaction with telomerase holoenzyme. *J. Biol. Chem.* **287**, 34455–34464 (2012). Medline doi:10.1074/jbc.M112.394767

11. J. Nandakumar, C. F. Bell, I. Weidenfeld, A. J. Zaug, L. A. Leinwand, T. R. Cech, The TEL patch of telomere protein TPP1 mediates telomerase recruitment and processivity. *Nature* **492**, 285–289 (2012). Medline doi:10.1038/nature11648

12. H. Xin, D. Liu, M. Wan, A. Safari, H. Kim, W. Sun, M. S. O'Connor, Z. Songyang, TPP1 is a homologue of ciliate TEBP-β and interacts with POT1 to recruit telomerase. *Nature* **445**, 559–562 (2007). Medline doi:10.1038/nature05469

13. F. Wang, E. R. Podell, A. J. Zaug, Y. Yang, P. Baciu, T. R. Cech, M. Lei, The POT1-TPP1 telomere complex is a telomerase processivity factor. *Nature* **445**, 506–510 (2007). Medline doi:10.1038/nature05454

14. T. Rao, J. W. Lubin, G. S. Armstrong, T. M. Tucey, V. Lundblad, D. S. Wuttke, Structure of Est3 reveals a bimodal surface with differential roles in telomere replication. *Proc. Natl. Acad. Sci. U.S.A.* **111**, 214–218 (2014). Medline doi:10.1073/pnas.1316453111

15. J. M. Talley, D. C. DeZwaan, L. D. Maness, B. C. Freeman, K. L. Friedman, Stimulation of yeast telomerase activity by the ever shorter telomere 3 (Est3) subunit is dependent on

direct interaction with the catalytic protein Est2. *J. Biol. Chem.* **286**, 26431–26439 (2011). Medline doi:10.1074/jbc.M111.228635

16. A. Prakash, G. E. Borgstahl, The structure and function of replication protein A in DNA replication. *Subcell. Biochem.* **62**, 171–196 (2012). Medline doi:10.1007/978-94-007-4572-8_10

17. K. A. Lewis, D. S. Wuttke, Telomerase and telomere-associated proteins: Structural insights into mechanism and evolution. *Structure* **20**, 28–39 (2012). Medline doi:10.1016/j.str.2011.10.017

18. L. Y. Chen, S. Redon, J. Lingner, The human CST complex is a terminator of telomerase activity. *Nature* **488**, 540–544 (2012). Medline doi:10.1038/nature11269

19. C. M. Price, K. A. Boltz, M. F. Chaiken, J. A. Stewart, M. A. Beilstein, D. E. Shippen, Evolution of CST function in telomere maintenance. *Cell Cycle* **9**, 3157–3165 (2010). Medline doi:10.4161/cc.9.16.12547

20. P. Wu, H. Takai, T. de Lange, Telomeric 3′ overhangs derive from resection by Exo1 and Apollo and fill-in by POT1b-associated CST. *Cell* **150**, 39–52 (2012). Medline doi:10.1016/j.cell.2012.05.026

21. F. Wang, J. A. Stewart, C. Kasbek, Y. Zhao, W. E. Wright, C. M. Price, Human CST has independent functions during telomere duplex replication and C-strand fill-in. *Cell Reports* **2**, 1096–1103 (2012). Medline doi:10.1016/j.celrep.2012.10.007

22. N. F. Lue, E. Y. Yu, M. Lei, A popular engagement at the ends. *Nat. Struct. Mol. Biol.* **20**, 10–12 (2013). Medline doi:10.1038/nsmb.2483

23. T. M. Tucey, V. Lundblad, Regulated assembly and disassembly of the yeast telomerase quaternary complex. *Genes Dev.* **28**, 2077–2089 (2014). Medline doi:10.1101/gad.246256.114

24. R. J. Wellinger, V. A. Zakian, Everything you ever wanted to know about *Saccharomyces cerevisiae* telomeres: Beginning to end. *Genetics* **191**, 1073–1105 (2012). Medline doi:10.1534/genetics.111.137851

25. E. D. Egan, K. Collins, Biogenesis of telomerase ribonucleoproteins. *RNA* **18**, 1747–1759 (2012). Medline doi:10.1261/rna.034629.112

26. J. D. Podlevsky, J. J. Chen, It all comes together at the ends: Telomerase structure, function, and biogenesis. *Mutat. Res.* **730**, 3–11 (2012). Medline doi:10.1016/j.mrfmmm.2011.11.002

27. H. E. Upton, K. Hong, K. Collins, Direct single-stranded DNA binding by Teb1 mediates the recruitment of *Tetrahymena thermophila* telomerase to telomeres. *Mol. Cell. Biol.* **34**, 4200–4212 (2014). Medline doi:10.1128/MCB.01030-14

28. B. Min, K. Collins, An RPA-related sequence-specific DNA-binding subunit of telomerase holoenzyme is required for elongation processivity and telomere maintenance. *Mol. Cell* **36**, 609–619 (2009). Medline doi:10.1016/j.molcel.2009.09.041

29. J. Jiang, E. J. Miracco, K. Hong, B. Eckert, H. Chan, D. D. Cash, B. Min, Z. H. Zhou, K. Collins, J. Feigon, The architecture of *Tetrahymena* telomerase holoenzyme. *Nature* **496**, 187–192 (2013). Medline doi:10.1038/nature12062

30. C. A. Theimer, J. Feigon, Structure and function of telomerase RNA. *Curr. Opin. Struct. Biol.* **16**, 307–318 (2006). Medline doi:10.1016/j.sbi.2006.05.005

31. A. J. Gillis, A. P. Schuller, E. Skordalakes, Structure of the *Tribolium castaneum* telomerase catalytic subunit TERT. *Nature* **455**, 633–637 (2008). Medline doi:10.1038/nature07283

32. S. A. Jacobs, E. R. Podell, T. R. Cech, Crystal structure of the essential N-terminal domain of telomerase reverse transcriptase. *Nat. Struct. Mol. Biol.* **13**, 218–225 (2006). Medline doi:10.1038/nsmb1054

33. M. Singh, Z. Wang, B. K. Koo, A. Patel, D. Cascio, K. Collins, J. Feigon, Structural basis for telomerase RNA recognition and RNP assembly by the holoenzyme La family protein p65. *Mol. Cell* **47**, 16–26 (2012). Medline doi:10.1016/j.molcel.2012.05.018

34. M. D. Stone, M. Mihalusova, C. M. O'connor, R. Prathapam, K. Collins, X. Zhuang, Stepwise protein-mediated RNA folding directs assembly of telomerase ribonucleoprotein. *Nature* **446**, 458–461 (2007). Medline doi:10.1038/nature05600

35. N. K. Jacob, R. Lescasse, B. R. Linger, C. M. Price, *Tetrahymena* POT1a regulates telomere length and prevents activation of a cell cycle checkpoint. *Mol. Cell. Biol.* **27**, 1592–1601 (2007). Medline doi:10.1128/MCB.01975-06

36. K. Hong, H. Upton, E. J. Miracco, J. Jiang, Z. H. Zhou, J. Feigon, K. Collins, *Tetrahymena* telomerase holoenzyme assembly, activation, and inhibition by domains of the p50 central hub. *Mol. Cell. Biol.* **33**, 3962–3971 (2013). Medline doi:10.1128/MCB.00792-13

37. S. Rouda, E. Skordalakes, Structure of the RNA-binding domain of telomerase: Implications for RNA recognition and binding. *Structure* **15**, 1403–1412 (2007). Medline doi:10.1016/j.str.2007.09.007

38. M. Mitchell, A. Gillis, M. Futahashi, H. Fujiwara, E. Skordalakes, Structural basis for telomerase catalytic subunit TERT binding to RNA template and telomeric DNA. *Nat. Struct. Mol. Biol.* **17**, 513–518 (2010). Medline doi:10.1038/nsmb.1777

39. N. F. Lue, Y. C. Lin, I. S. Mian, A conserved telomerase motif within the catalytic domain of telomerase reverse transcriptase is specifically required for repeat addition processivity. *Mol. Cell. Biol.* **23**, 8440–8449 (2003). Medline doi:10.1128/MCB.23.23.8440-8449.2003

40. M. Xie, J. D. Podlevsky, X. Qi, C. J. Bley, J. J. Chen, A novel motif in telomerase reverse transcriptase regulates telomere repeat addition rate and processivity. *Nucleic Acids Res.* **38**, 1982–1996 (2010). Medline doi:10.1093/nar/gkp1198

41. R. A. Wu, K. Collins, Human telomerase specialization for repeat synthesis by unique handling of primer-template duplex. *EMBO J.* **33**, 921–935 (2014). Medline doi:10.1002/embj.201387205

42. B. Eckert, K. Collins, Roles of telomerase reverse transcriptase N-terminal domain in assembly and activity of *Tetrahymena* telomerase holoenzyme. *J. Biol. Chem.* **287**, 12805–12814 (2012). Medline doi:10.1074/jbc.M112.339853

43. F. Qiao, T. R. Cech, Triple-helix structure in telomerase RNA contributes to catalysis. *Nat. Struct. Mol. Biol.* **15**, 634–640 (2008). Medline doi:10.1038/nsmb.1420

44. D. D. Cash, O. Cohen-Zontag, N. K. Kim, K. Shefer, Y. Brown, N. B. Ulyanov, Y. Tzfati, J. Feigon, Pyrimidine motif triple helix in the *Kluyveromyces lactis* telomerase RNA pseudoknot is essential for function in vivo. *Proc. Natl. Acad. Sci. U.S.A.* **110**, 10970–10975 (2013). Medline doi:10.1073/pnas.1309590110

45. C. A. Theimer, C. A. Blois, J. Feigon, Structure of the human telomerase RNA pseudoknot reveals conserved tertiary interactions essential for function. *Mol. Cell* **17**, 671–682 (2005). Medline doi:10.1016/j.molcel.2005.01.017

46. M. Mihalusova, J. Y. Wu, X. Zhuang, Functional importance of telomerase pseudoknot revealed by single-molecule analysis. *Proc. Natl. Acad. Sci. U.S.A.* **108**, 20339–20344 (2011). Medline doi:10.1073/pnas.1017686108

47. C. M. O'Connor, K. Collins, A novel RNA binding domain in *Tetrahymena* telomerase p65 initiates hierarchical assembly of telomerase holoenzyme. *Mol. Cell. Biol.* **26**, 2029–2036 (2006). Medline doi:10.1128/MCB.26.6.2029-2036.2006

48. A. J. Berman, A. R. Gooding, T. R. Cech, *Tetrahymena* telomerase protein p65 induces conformational changes throughout telomerase RNA (TER) and rescues telomerase reverse transcriptase and TER assembly mutants. *Mol. Cell. Biol.* **30**, 4965–4976 (2010). Medline doi:10.1128/MCB.00827-10

49. X. Qi, M. Xie, A. F. Brown, C. J. Bley, J. D. Podlevsky, J. J. Chen, RNA/DNA hybrid binding affinity determines telomerase template-translocation efficiency. *EMBO J.* **31**, 150–161 (2012). Medline doi:10.1038/emboj.2011.363

50. Z. Zeng, B. Min, J. Huang, K. Hong, Y. Yang, K. Collins, M. Lei, Structural basis for *Tetrahymena* telomerase processivity factor Teb1 binding to single-stranded telomeric-repeat DNA. *Proc. Natl. Acad. Sci. U.S.A.* **108**, 20357–20361 (2011). Medline doi:10.1073/pnas.1113624108

51. E. Bochkareva, S. Korolev, S. P. Lees-Miller, A. Bochkarev, Structure of the RPA trimerization core and its role in the multistep DNA-binding mechanism of RPA. *EMBO J.* **21**, 1855–1863 (2002). Medline doi:10.1093/emboj/21.7.1855

52. S. F. Altschul, T. L. Madden, A. A. Schäffer, J. Zhang, Z. Zhang, W. Miller, D. J. Lipman, Gapped BLAST and PSI-BLAST: A new generation of protein database search programs. *Nucleic Acids Res.* **25**, 3389–3402 (1997). Medline doi:10.1093/nar/25.17.3389

53. C. Cole, J. D. Barber, G. J. Barton, The Jpred 3 secondary structure prediction server. *Nucleic Acids Res.* **36** (suppl. 2), W197–W201 (2008). Medline doi:10.1093/nar/gkn238

54. B. Min, K. Collins, Multiple mechanisms for elongation processivity within the reconstituted *Tetrahymena* telomerase holoenzyme. *J. Biol. Chem.* **285**, 16434–16443 (2010). Medline doi:10.1074/jbc.M110.119172

55. J. Xiong, X. Lu, Z. Zhou, Y. Chang, D. Yuan, M. Tian, Z. Zhou, L. Wang, C. Fu, E. Orias, W. Miao, Transcriptome analysis of the model protozoan, *Tetrahymena thermophila*, using deep RNA sequencing. *PLOS ONE* **7**, e30630 (2012). Medline doi:10.1371/journal.pone.0030630

56. A. N. Sexton, S. G. Regalado, C. S. Lai, G. J. Cost, C. M. O'Neil, F. D. Urnov, P. D. Gregory, R. Jaenisch, K. Collins, D. Hockemeyer, Genetic and molecular identification of three human TPP1 functions in telomerase action: Recruitment, activation, and homeostasis set point regulation. *Genes Dev.* **28**, 1885–1899 (2014). Medline

57. J. C. Schmidt, A. B. Dalby, T. R. Cech, Identification of human TERT elements necessary for telomerase recruitment to telomeres. *eLife* **3**, e03563 (2014). doi:10.7554/eLife.03563

58. J. Sun, E. Y. Yu, Y. Yang, L. A. Confer, S. H. Sun, K. Wan, N. F. Lue, M. Lei, Stn1-Ten1 is an Rpa2-Rpa3-like complex at telomeres. *Genes Dev.* **23**, 2900–2914 (2009). Medline doi:10.1101/gad.1851909

59. C. Bryan, C. Rice, M. Harkisheimer, D. C. Schultz, E. Skordalakes, Structure of the human telomeric Stn1-Ten1 capping complex. *PLOS ONE* **8**, e66756 (2013). Medline doi:10.1371/journal.pone.0066756

60. B. Vester, J. Wengel, LNA (locked nucleic acid): High-affinity targeting of complementary RNA and DNA. *Biochemistry* **43**, 13233–13241 (2004). Medline doi:10.1021/bi0485732

61. J. Huang, A. F. Brown, J. Wu, J. Xue, C. J. Bley, D. P. Rand, L. Wu, R. Zhang, J. J. Chen, M. Lei, Structural basis for protein-RNA recognition in telomerase. *Nat. Struct. Mol. Biol.* **21**, 507–512 (2014). Medline doi:10.1038/nsmb.2819

62. J. L. Chen, K. K. Opperman, C. W. Greider, A critical stem-loop structure in the CR4-CR5 domain of mammalian telomerase RNA. *Nucleic Acids Res.* **30**, 592–597 (2002). Medline doi:10.1093/nar/30.2.592

63. C. J. Bley, X. Qi, D. P. Rand, C. R. Borges, R. W. Nelson, J. J. Chen, RNA-protein binding interface in the telomerase ribonucleoprotein. *Proc. Natl. Acad. Sci. U.S.A.* **108**, 20333–20338 (2011). Medline doi:10.1073/pnas.1100270108

64. A. J. Zaug, E. R. Podell, T. R. Cech, Mutation in TERT separates processivity from anchor-site function. *Nat. Struct. Mol. Biol.* **15**, 870–872 (2008). Medline doi:10.1038/nsmb.1462

65. B. R. Linger, G. B. Morin, C. M. Price, The Pot1a-associated proteins Tpt1 and Pat1 coordinate telomere protection and length regulation in *Tetrahymena*. *Mol. Biol. Cell* **22**, 4161–4170 (2011). Medline doi:10.1091/mbc.E11-06-0551

66. C. Suloway, J. Pulokas, D. Fellmann, A. Cheng, F. Guerra, J. Quispe, S. Stagg, C. S. Potter, B. Carragher, Automated molecular microscopy: The new Leginon system. *J. Struct. Biol.* **151**, 41–60 (2005). Medline doi:10.1016/j.jsb.2005.03.010

67. X. Li, P. Mooney, S. Zheng, C. R. Booth, M. B. Braunfeld, S. Gubbens, D. A. Agard, Y. Cheng, Electron counting and beam-induced motion correction enable near-atomic-resolution single-particle cryo-EM. *Nat. Methods* **10**, 584–590 (2013). Medline doi:10.1038/nmeth.2472

68. J. A. Mindell, N. Grigorieff, Accurate determination of local defocus and specimen tilt in electron microscopy. *J. Struct. Biol.* **142**, 334–347 (2003). Medline doi:10.1016/S1047-8477(03)00069-8

69. J. B. Heymann, D. M. Belnap, Bsoft: Image processing and molecular modeling for electron microscopy. *J. Struct. Biol.* **157**, 3–18 (2007). Medline doi:10.1016/j.jsb.2006.06.006

70. N. R. Voss, C. K. Yoshioka, M. Radermacher, C. S. Potter, B. Carragher, DoG Picker and TiltPicker: Software tools to facilitate particle selection in single particle electron microscopy. *J. Struct. Biol.* **166**, 205–213 (2009). Medline doi:10.1016/j.jsb.2009.01.004

71. S. J. Ludtke, P. R. Baldwin, W. Chiu, EMAN: Semiautomated software for high-resolution single-particle reconstructions. *J. Struct. Biol.* **128**, 82–97 (1999). Medline doi:10.1006/jsbi.1999.4174

72. S. H. Scheres, RELION: Implementation of a Bayesian approach to cryo-EM structure determination. *J. Struct. Biol.* **180**, 519–530 (2012). Medline doi:10.1016/j.jsb.2012.09.006

73. E. F. Pettersen, T. D. Goddard, C. C. Huang, G. S. Couch, D. M. Greenblatt, E. C. Meng, T. E. Ferrin, UCSF Chimera—A visualization system for exploratory research and analysis. *J. Comput. Chem.* **25**, 1605–1612 (2004). Medline doi:10.1002/jcc.20084

74. A. Kucukelbir, F. J. Sigworth, H. D. Tagare, Quantifying the local resolution of cryo-EM density maps. *Nat. Methods* **11**, 63–65 (2014). Medline doi:10.1038/nmeth.2727

75. P. Emsley, K. Cowtan, *Coot*: Model-building tools for molecular graphics. *Acta Crystallogr. D* **60**, 2126–2132 (2004). Medline doi:10.1107/S0907444904019158

76. P. Chacón, W. Wriggers, Multi-resolution contour-based fitting of macromolecular structures. *J. Mol. Biol.* **317**, 375–384 (2002). Medline doi:10.1006/jmbi.2002.5438

77. The PyMOL Molecular Graphics System, Version 1.7.4, Schrödinger, LLC.

78. A. F. Moon, G. A. Mueller, X. Zhong, L. C. Pedersen, A synergistic approach to protein crystallization: Combination of a fixed-arm carrier with surface entropy reduction. *Protein Sci.* **19**, 901–913 (2010). Medline

79. K. L. Witkin, K. Collins, Holoenzyme proteins required for the physiological assembly and activity of telomerase. *Genes Dev.* **18**, 1107–1118 (2004). Medline doi:10.1101/gad.1201704

80. W. Kabsch, Integration, scaling, space-group assignment and post-refinement. *Acta Crystallogr. D* **66**, 133–144 (2010). Medline doi:10.1107/S0907444909047374

81. A. J. McCoy, R. W. Grosse-Kunstleve, P. D. Adams, M. D. Winn, L. C. Storoni, R. J. Read, *Phaser* crystallographic software. *J. Appl. Cryst.* **40**, 658–674 (2007). Medline doi:10.1107/S0021889807021206

82. P. V. Afonine, R. W. Grosse-Kunstleve, N. Echols, J. J. Headd, N. W. Moriarty, M. Mustyakimov, T. C. Terwilliger, A. Urzhumtsev, P. H. Zwart, P. D. Adams, Towards automated crystallographic structure refinement with *phenix.refine*. *Acta Crystallogr. D* **68**, 352–367 (2012). Medline doi:10.1107/S0907444912001308

83. N. K. Kim, Q. Zhang, J. Zhou, C. A. Theimer, R. D. Peterson, J. Feigon, Solution structure and dynamics of the wild-type pseudoknot of human telomerase RNA. *J. Mol. Biol.* **384**, 1249–1261 (2008). Medline doi:10.1016/j.jmb.2008.10.005

84. J. Erde, R. R. Loo, J. A. Loo, Enhanced FASP (eFASP) to increase proteome coverage and sample recovery for quantitative proteomic experiments. *J. Proteome Res.* **13**, 1885–1895 (2014). Medline doi:10.1021/pr4010019

85. R. J. Richards, H. Wu, L. Trantirek, C. M. O'Connor, K. Collins, J. Feigon, Structural study of elements of *Tetrahymena* telomerase RNA stem-loop IV domain important for function. *RNA* **12**, 1475–1485 (2006). Medline doi:10.1261/rna.112306

86. R. J. Richards, C. A. Theimer, L. D. Finger, J. Feigon, Structure of the *Tetrahymena thermophila* telomerase RNA helix II template boundary element. *Nucleic Acids Res.* **34**, 816–825 (2006). Medline doi:10.1093/nar/gkj481

87. O. Kotik-Kogan, E. R. Valentine, D. Sanfelice, M. R. Conte, S. Curry, Structural analysis reveals conformational plasticity in the recognition of RNA 3′ ends by the human La protein. *Structure* **16**, 852–862 (2008). Medline doi:10.1016/j.str.2008.02.021

88. J. Fan, N. P. Pavletich, Structure and conformational change of a replication protein A heterotrimer bound to ssDNA. *Genes Dev.* **26**, 2337–2347 (2012). Medline doi:10.1101/gad.194787.112